Electronic Materials Letters, Vol. 9, No. 2 (2013), pp. 171-176
DOI: 10.1007/s13391-012-2170-3

Influence of Solution Concentrations on Surface Morphology and Wettability of ZnO Thin Films

Jianguo Lv,[1,2,3] Changlong Liu,[2] Feng Wang,[2] Zhitao Zhou,[2] Zhenfa Zi,[2] Yuan Feng,[2,*] Xiaoshuang Chen,[3,*] Feng Liu,[4] Gang He,[1] Shiwei Shi,[1] Xueping Song,[1] and Zhaoqi Sun[1,*]

[1]School of Physics and Material Science, Anhui University, Hefei 230039, China
[2]School of Electronic and Information Engineering, Hefei Normal University, Hefei 230061, China
[3]National Laboratory for Infrared Physics, Shanghai Institute of Technical Physics, Chinese Academy of Sciences, Shanghai 200083, China
[4]School of Mathematics and Physics, Anhui Polytechnic University, Wuhu 241000, China

(received date: 24 September 2012 / accepted date: 3 December 2012 / published date: March 2013)

ZnO thin films were grown on silicon substrates using a hydrothermal method. The XRD patterns show that all of the peaks can be attributed to the wurtzite structures of ZnO. The *TC* value of (002) plane and average crystal size increase first and then decrease with the increase of solution concentration. SEM and AFM results show that many dense hexagonal cylinder particles have been observed on the surface of the thin films, which grown at 0.08 and 0.10 mol/L. The surface roughness of the thin films deposited at 0.06, 0.08, 0.10, and 0.12 mol/L are 24.5, 38.3, 32.0, and 39.4 nm, respectively. Surface wettability results show that the preferential orientation along *c*-axis and surface roughness contribute significantly to the hydrophobicity. The reversible switching between hydrophobicity and hydrophilicity is related to the synergy of the transition of wetting model, surface crystal structure, and surface roughness.

Keywords: ZnO thin films, solution concentrations, wettability, crystal structure

1. INTRODUCTION

During the past decade there has been an increasing interest in controlling the wettability of solids, which depends on the surface free energy as well as the geometric structures of the surface. Functional surfaces that can be reversibly switched between hydrophobicity and hydrophilicity under the external stimuli have aroused great interest due to a wide range of potential applications, including self-cleaning surfaces, controllable drug delivery, microreactors and laboratory-on-chip devices.[1-4] So far, many studies have been carried out on the wetting behaviors of nanomaterials based on metal oxides. Among these metal oxides materials, ZnO nanostructures have been used to generate hydrophobic surface because of the minimum water-solid contact fraction of this sort of structures. The wettability conversion phenomenon of ZnO also can be achieved by ultraviolet (UV) illumination.[5-7] So far, a variety of fabrication methods, such as pulsed laser deposition,[8] sol-gel technique,[9] chemical vapor deposition,[10] electrochemical deposition[11] and hydrothermal method,[12] have been used to create hydrophobic ZnO nanostructures. Among these methods, hydrothermal method offers an efficient way to generate ZnO nanostructures due to low cost, simplicity and low temperature growth. So far, previous works have been focused mainly on ZnO nanorods, nanowires, and nanobelts. However, the remaining challenge is to develop simple and reliable synthetic methods for ZnO hierarchical architectures, which are important to explore in detail the effect of morphology on wettability.

In this letter, effect of solution concentration on ZnO thin films, which deposited by a hydrothermal technique, has been investigated. The photo-induced reversible wetting properties of ZnO thin films with different nanostructures were studied in detail. Mechanism of photo-induced transition between two distinct wetting states has been discussed.

2. EXPERIMENTAL PROCEDURE

ZnO thin films were grown on ZnO seed layers, which were prepared by a sol-gel method, using a hydrothermal technique. The synthesis details of ZnO seed layers can be found in our previous paper.[13] The ZnO thin films were grown by suspending the ZnO seed layers vertically in a 50 mL Teflon-lined stainless steel autoclave filled with

*Corresponding author: yfeng@iccas.ac.cn
*Corresponding author: szq@ahu.edu.cn
*Corresponding author: xschen@mail.sitp.ac.cn

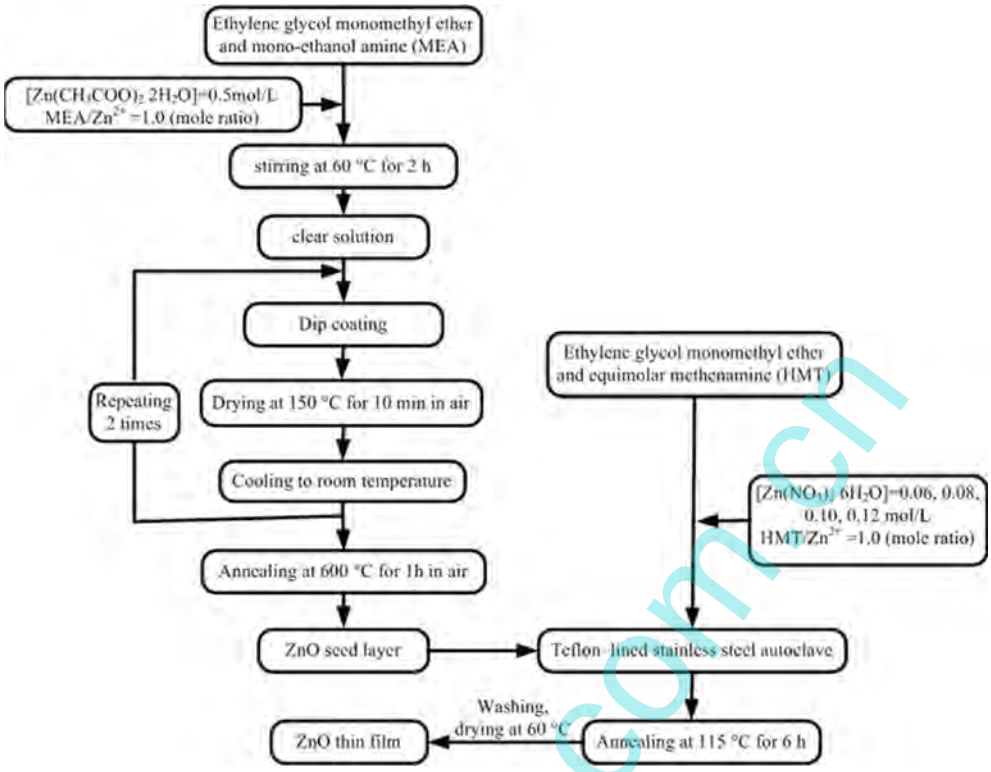

Fig. 1. Schematic diagram of the procedure for preparing ZnO thin films.

40 mL ethylene glycol monomethyl ether solution of zinc nitrate hexahydrate [$Zn(NO_3)_2$ $6H_2O$] and equimolar methenamine ($C_6H_{12}N_4$, HMT) at 115°C for 6 h in an oven. The concentrations of zinc nitrate hexahydrate and HMT were 0.06, 0.08, 0.10 and 0.12 mol/L, respectively. After growth, the samples were taken out from the solution, rinsed with deionized water and dried at room temperature for further characterization. The schematic diagram of the procedure for preparing ZnO thin films is given in Fig. 1. Average thickness of the sample deposited at 0.10 mol/L was determined to be 458 nm by using AMBIOS XP-1 profilometer.

The microstructure of the ZnO thin film was examined by x-ray diffractometry (XRD, BRUKER D8 Advance). The surface morphology of the ZnO thin film was investigated using field-emission scanning electron microscopy (FE-SEM, HITACHI S-4800) and atomic force microscopy (AFM, CSPM4000). The static water contact angles (WCAs) on the ZnO thin films were measured at room temperature using a home-made water contact angle apparatus. The volume of the water droplets used for the static WCA measurements was 5 μL. Four water droplets were placed at different locations on a horizontal surface, and the mean value was reported. Photo-induced hydrophilicity was measured by irradiating the samples at certain time intervals using a low pressure mercury lamp (λ = 365 nm) with an intensity of 1 $\mu W/cm^{-2}$. After each irradiation time interval, a 5 μL water droplet was placed on the irradiated area and the corresponding contact angle was measured. The typical error of the WCA measurement is ±1°.

3. RESULTS AND DISCUSSION

The XRD spectra of ZnO thin films deposited at different solution concentrations on silicon substrates are shown in Fig. 2. It is well seen from the spectra that all peaks can be indexed to the wurtzite structures of ZnO (JCPDS Card No. 36-1451), and no other impurity phase was found. Crystallinity and preferential orientation depend on the solution concentrations. In order to obtain the quantitative information concerning the preferential crystalline orientation, the texture coefficient $TC_{(hkl)}$ has been calculated by using the following relation:[14]

$$TC_{(hkl)} = \frac{I_{(hkl)}/I_{0(hkl)}}{\frac{1}{N}\sum_{N} I_{(hkl)}/I_{0(hkl)}} \quad (1)$$

where $I_{(hkl)}$ is the measured relative intensity of the *(hkl)* plane, $I_{0(hkl)}$ is the standard intensity of the *(hkl)* plane taken from the JCPDS 36-1451 data, and N is the total number of reflection peaks from the thin film. In the present letter, n = 5 because five major reflection peaks come from (*100*), (*002*), (*101*), (*102*), and (*110*) plane are involved. The value, $TC_{(hkl)}$ = 1, represents the thin film with randomly oriented crystallites,

while higher value indicates the abundance of crystallites oriented along *(hkl)* direction. The variations of *TC* for ZnO thin films deposited at different solution concentrations are listed in Table 1. It can be seen that the *TC* value of (*002*) plane of ZnO thin films deposited at 0.06 mol/L is less than 1. The *TC* value of (*002*) plane increases to a maximum at 0.10 mol/L and then decreases with the increase of solution concentration. The result indicates that many hexagonal cylinder particles grown along *c*-axis perpendicular to the substrate surface when the solution concentration is 0.10 mol/L.

The crystal size of thin films was calculated using the well-known Scherrer's formula:[15]

$$D = \frac{0.9\lambda}{\beta\cos\theta} \quad (2)$$

where D is the crystal size of the thin film, λ (= 0.15406 nm) is the wavelength of the x-ray used, β is the full width at half maximum (FWHM) and θ is the angle of diffraction. The calculated values of the average crystal size are listed in Table 1. It can be seen that the crystallinity improves first and then reduces with the increase of solution concentration.

Typical FE-SEM images of ZnO thin films with different solution concentrations from 0.06 to 0.12 mol/L are shown in Fig. 3. It can be seen that the solution concentrations have great influence on the thin film surface morphology. When the solution concentration is 0.06 mol/L, sparse hexagonal cylinder particles were observed and distributed randomly over whole thin film surface. The result can be explained that nuclei that are formed in ethylene glycol monomethyl ether solution can aggregate into small ZnO particles due to the low zinc nitrate concentration. These particles may serve as seed for thin films growth. Some hexagonal cylinder particles were elongated on *c*-axis, but they were laid on the substrate. So, the relative intensity of the diffraction peaks of the thin film is similar to that of the JCPDS data, showing a random growth of particles. Length and diameter of hexagonal cylinder particles increase with the increases of solution concentration. When the solution concentration increases to 0.08 and 0.10 mol/L, many dense hexagonal cylinder particles tend to grow perpendicular to the substrate surface. As the concentration increases, larger nuclei are obtained in the solution, forming much larger ZnO seeds, greatly promoting the formation of larger ZnO nanoparticles. It can be seen from Fig. 2 that the intensity of (*002*) diffraction peak of the thin films at 0.08 mol/L and 0.10 mol/L is much higher than that of other diffraction peaks. High intensity of (*002*) diffraction peak would be caused by many hexagonal cylinder particles grown on the substrate with their *c*-axis perpendicular to the substrate surface. With a further increase in the solution concentration, density of the thin films increases but the hexagonal cylinder particles have been damaged. Many small holes and large cracks, which lead to the decrease of relative intensity of (*002*) diffraction peak, have been observed on the hexagonal cylinder particles of ZnO thin film with solution concentration of 0.12 mol/L.

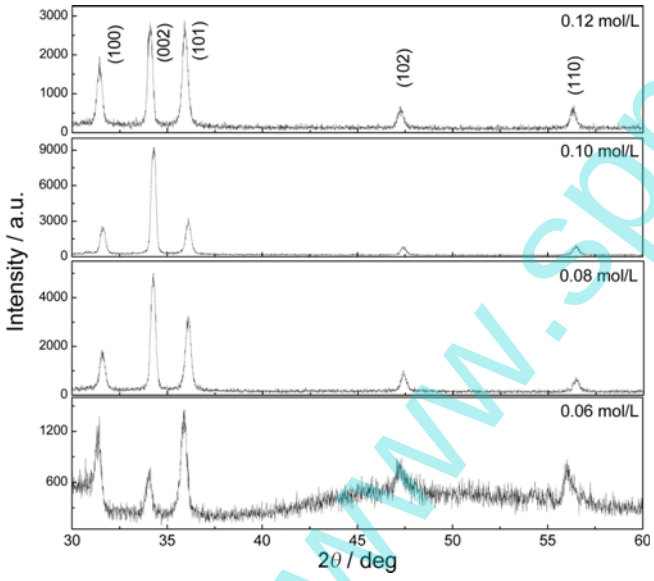

Fig. 2. XRD pattern of ZnO thin film deposited at different solution concentration.

Figure 4 shows the AFM images of ZnO thin films deposited at different solution concentrations. The images are obtained in contacting mode taken over a scale of 5 μm × 5 μm. The rms roughness of the thin films deposited at 0.06, 0.08, 0.10, and 0.12 mol/L are 24.5, 38.3, 32.0, and 39.4 nm, respectively.

Surface wettability is a very important property governed by both the surface free energy and the surface roughness of solid surfaces. In order to fully utilize the wettability of nanostructured surfaces, it is necessary to study the fundamental

Table 1. Values of texture coefficient and crystal size of ZnO thin film deposited at different solution concentrations.

Solution concentration (mol/L)	Texture coefficient (*TC*)					Crystal size (nm)
	$TC_{(100)}$	$TC_{(002)}$	$TC_{(101)}$	$TC_{(102)}$	$TC_{(110)}$	
0.06	1.224	0.838	0.702	1.419	0.817	26.6
0.08	0.828	2.495	0.677	0.681	0.320	37.5
0.10	0.747	3.118	0.439	0.422	0.274	42.1
0.12	1.055	1.992	0.847	0.661	0.445	36.1

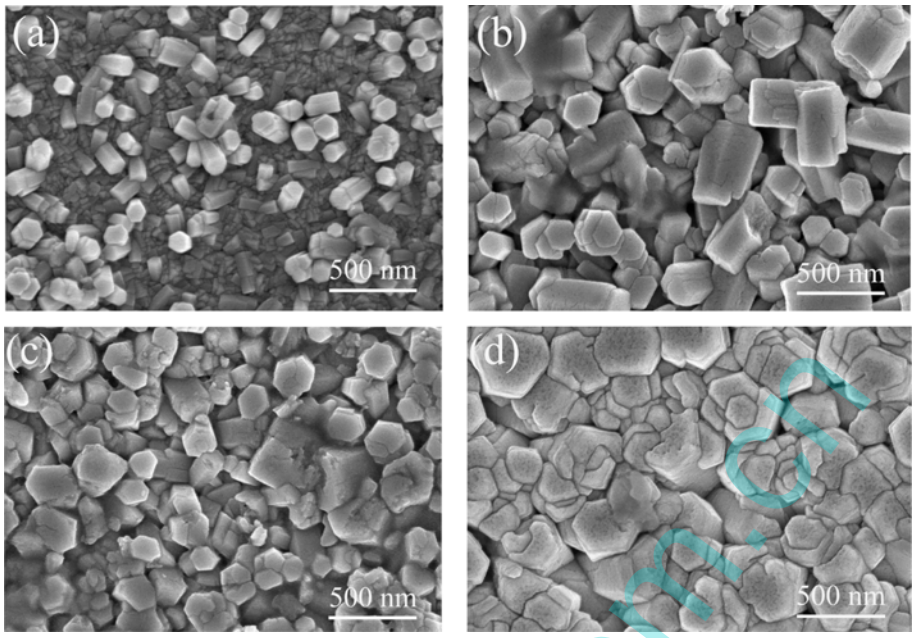

Fig. 3. FE-SEM images of ZnO thin films grown using different zinc nitrate concentrations (a) 0.06 mol/L, (b) 0.08 mol/L, (c) 0.10 mol/L, and (d) 0.12 mol/L.

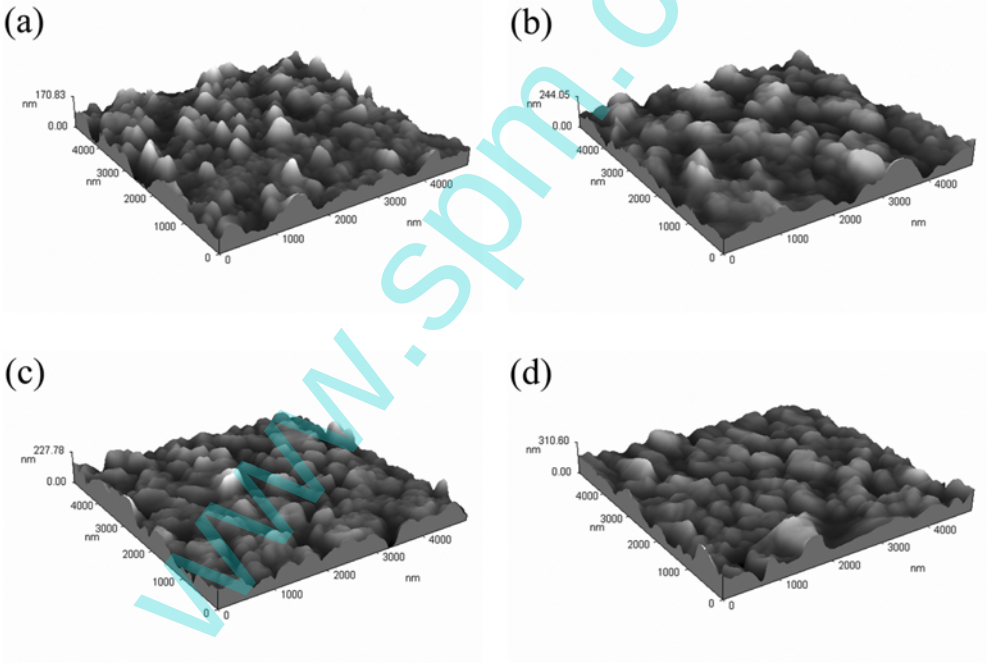

Fig. 4. AFM images of ZnO thin films deposited at different solution concentrations: (a) 0.06 mol/L, (b) 0.08 mol/L, (c) 0.10 mol/L, and (d) 0.12 mol/L.

relationship between the different nanostructure and the wettability. Surface wettability is evaluated using water contact angle (WCA) measurement. The shapes of 5 μL water droplets on the surfaces are shownin Fig. 5(a), (c), (e) and (g). The WCA values of the ZnO thin films deposited at different solution concentration are listed in Table 2. It is well known that the surface roughness may amplify the present wettability character. Hydrophobicity would be enhanced via surface roughening when the liquid does not completely permeate the low surface energy material. Therefore, the wetting behavior of the thin film in this letter can be described by the Cassie-Baxter model as follow:

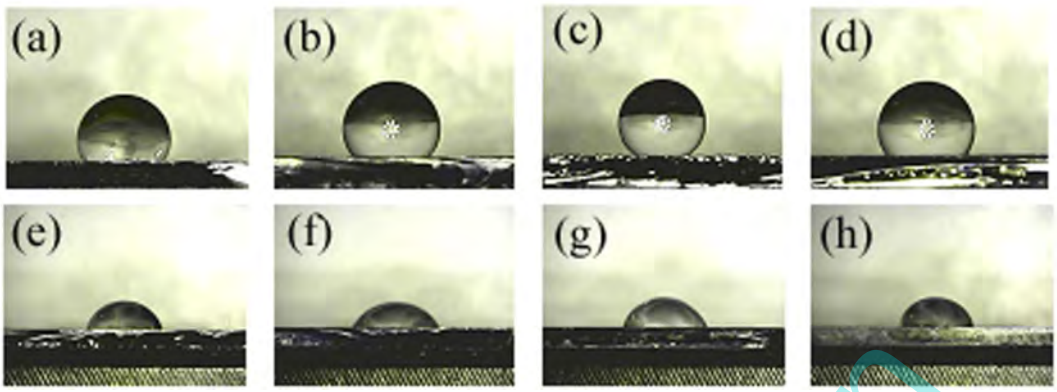

Fig. 5. Water contact angle images of ZnO thin films grown at (a) and (e) 0.06 mol/L, (b) and (f) 0.08 mol/L, (c) and (g) 0.10 mol/L, and (d) and (h) 0.012 mol/L, before and after illumination, respectively.

Table 2. Water contact angle before and after 120 min of UV irradiation and roughness of ZnO deposited at different solution concentration.

Solution concentration (mol/L)	Water contact angle (°)		Roughness value (nm)
	before UV irradiation	after 120 min of UV irradiation	
0.06	113	74	24.5
0.08	124	59	38.3
0.10	140	75	32.0
0.12	121	78	39.4

$$\cos\theta_{CB} = f(1+\cos\theta) - 1 \quad (3)$$

where f is the fraction of the projected solid surface. As f is always lower than unity, this model always predicts enhancement of hydrophobicity only, independent of the value of the initial contact angle. It can be seen from Table 2 that the WCAs of all the thin films higher than 90° and the WCA increases first, reach its maximum at 0.10 mol/L, and then decrease with the increase of solution concentration. The change of the WCA can be attributed to a synergistic effect of preferential orientation along the *c*-axis and surface roughness.[12]

Regarding the photo-induced transition of the wettability of the ZnO thin films, Fig. 5(b), (d), (f) and (h) present the water contact angle images after an exposure to UV irradiation for 120 min. The corresponding WCA values are listed in Table 2. It can be seen that all the samples exhibit obvious photo-induced transition in their wettability to hydrophilicity. The contact angle reduction rate,[12] which can be used to describe the relative changes of photo-induced hydrophilicity, is 0.655, 0.476, 0.536, and 0.645, respectively. The smaller contact angle reduction rate is, the larger the change of contact angle is. The results indicate that the maximum photo-induced transition has been observed in the ZnO thin film deposited at 0.08 mol/L. The change of the wettability characteristic can be explained as follow:

By UV light irradiation with photon energy, higher than or equal to the band gap of ZnO, the electrons in the valence band are excited to the conduction band. The same numbers of holes are simultaneously generated in the valence band.[16] Some of the holes react with lattice oxygen to form surface oxygen vacancies, while the electrons can react with the metal ions (Zn^{2+}) present in the lattice, forming Zn^{+} defective sites. Meanwhile, water and oxygen may compete to dissociatively adsorb on these vacancies. The defective sites are kinetically more favorable for hydroxyl adsorption than oxygen adsorption. As a result, the surface hydrophilicity is improved, and the water contact angle can significantly be reduced.[8]

The photo-induced transition from hydrophobic to hydrophilic state is followed by the change of the Cassie-Baxter model to the Wenzel model. It is reasonable to conclude that after UV irradiation the liquid begins to penetrate the interstitial spaces between nanoparticles of the ZnO thin films, leading to the rapid decrease of contact angle. Therefore, the change of model promotes the hydrophilicity of the ZnO thin films. Moreover, the Wenzel model can be used to predict the possibility of superhydrophilicity of the thin film with very rough surfaces. This may be attributed to more photoactive defect sites, which are in contact with water molecules, on the very rough surfaces of the thin films. Thus, hydrophilicity of the ZnO thin films can be enhanced by increasing the surface roughness. The surface crystal structure also plays an important role in the photo-induced process. It has been reported that the change of contact angle of nonpolar planes oriented ZnO thin films is larger than those of polar planes oriented ZnO thin films.[17] The more ZnO thin films grow along the *c*-axis, the more nonpolar on the surface is. That is the reason of ZnO thin film with high proportion of nonpolar planes and large surface roughness grown at 0.08 mol/L has the maximum contact angle

transition. So, the variation of contact angle reduction rate can be ascribed to the transition of wetting model, surface roughness and surface crystal structure of ZnO thin films.

It should be pointed to that after storing the samples in dark at RT for several days, the hydrophilic surfaces could recover to their original hydrophobic state. This is due to the fact that the surface becomes energetically unstable after the hydroxyl adsorption. Since the oxygen adsorption is thermodynamically favored, oxygen is more strongly bonded on the defect sites than the hydroxyl group.[18] Therefore, the hydroxyl groups adsorbed on the defective sites can be replaced gradually by oxygen atoms when the UV-irradiated samples are stored in dark. As a result, the surface evolves back to its original state (before UV irradiation), and the wettability is reconverted from hydrophilicity to hydrophobicity again.[19]

4. CONCLUSIONS

Microstructure, surface topography and wettability of ZnO thin films deposited at different solution concentrations were measured by XRD, FE-SEM, AFM and home-made water contact angle apparatus. Effect of solution concentration on preferential orientation along the *c*-axis, average crystal size and surface roughness has been studied in detail. Effect of surface morphology and surface crystal structure on the wettability of ZnO thin films has been investigated. The change of the WCA before UV irradiation may be connected with the variation preferential orientation along the *c*-axis and surface roughness. The hydrophobicity states of the ZnO thin films were found to be converted to hydrophilicity after an exposure to UV irradiation for 120 min. This is explained by the semiconductor nature of ZnO thin films. The contact angle reduction rate of ZnO thin films depend strongly on the surface crystal structure and surface roughness.

ACKNOWLEDGEMENTS

This work was supported by National Natural Science Foundation of China (Nos. 51072001, 51272001, 51002156, 51272001 51102072), China Postdoctoral Science Foundation (No. 2012M520944), Anhui Provincial Natural Science Foundation (No. 1208085MF99, 1208085QA16), Shanghai Postdoctoral Science Foundation (Nos. 12R21416800), Natural Science Foundation of Anhui Higher Education Institution of China (No. KJ2010B148), Funds for Distinguished Young Scholar of Anhui University (No. KJJQ1103).

REFERENCES

1. O. D. Velev, B. G. Prevo, and K. H. Bhatt, *Nature* **426**, 515 (2003).
2. N. Verplanck, Y. Coffinier, V. Thomy, and R. Boukherroub, *Nanoscale Res. Lett.* **2**, 577 (2007).
3. Z. Guo, F. Zhou, J. Hao, and W. Liu, *J. Am. Chem. Soc.* **127**, 15670 (2005).
4. V. Zorba, E. Stratakis, M. Barberoglou, E. Spanakis, P. Tzanetakis, S. H. Anastasiadis, and C. Fotakis, *Adv. Mater.* **20**, 4049 (2008).
5. X. Feng, L. Feng, M. Jin, J. Zhai, L. Jiang, and D. Zhu, *J. Am. Chem. Soc.* **126**, 62 (2004).
6. G. Kenanakis, E. Stratakis, K. Vlachou, D. Vernardou, E. Koudoumas, and N. Katsarakis, *Appl. Surf. Sci.* **254**, 5695 (2008).
7. E. L. Papadopoulou, M. Barberoglou, V. Zorba, A. Manousaki, A. Pagkozidis, E. Stratakis, and C. Fotakis, *J. Phys. Chem. C* **113**, 2891 (2009).
8. E. L. Papadopoulou, V. Zorba, A. Pagkozidis, M. Barberoglou, E. Stratakis, and C. Fotakis, *Thin Solid Films* **518**, 1267 (2009).
9. X. H. Li, G. M. Chen, Y. M. Ma, L. Feng, H. Z. Zhao, L. Jiang, and F. S. Wang, *Polymer* **47**, 506 (2006).
10. L. Huang, S. P. Lau, H. Y. Yang, E. S. P. Leong, S. F. Yu, and S. Prawer, *J. Phys. Chem. B* **109**, 7746 (2005).
11. C. H. Wang, Y. Y. Song, and J. W. Zhao, *Surf. Sci.* **600**, 38 (2006).
12. J. Lv, C. Liu, W. Gong, Z. Zi, X. Chen, K. Huang, T. Wang, G. He, X. Song, and Z. Sun, *Sci. Adv. Mater.* **4**, 757 (2012).
13. J. Lv, C. Liu, W. Gong, Z. Zi, X. Chen, K. Huang, T. Wang, G. He, X. Song, and Z. Sun, *Superlattice. Microst.* **51**, 886 (2012).
14. S. Lemlikchi, S. Abdelli-Messaci, S. Lafane, T. Kerdja, A. Guittoum, and M. Saad, *Appl. Surf. Sci.* **256**, 5650 (2010).
15. J. G. Chen, C. X. Guo, L. L. Zhang, and J. T. Hu, *Chinese Phys. Lett.* **21**, 1366 (2004).
16. E. Spanakis, E. Stratakis, P. Tzanetakis, H. Fritzsche, S. Guha, and J. Yang, *J. Non-Cryst. Solids* **521**, 299 (2002).
17. M. Miyauchi, A. Shimai, and Y. Tsuru, *J. Phys. Chem. B* **109**, 13307 (2005).
18. G. Kenanakis, D. Vernardou, and N. Katsarakis, *Appl. Catal. A: Gen* **411-412**, 7 (2012).
19. M. Miyauchi, N. Kieda, S. Hishita, T. Mitsuhashi, A. Nakajima, T. Watanabe, and K. Hashimoto, *Surf. Sci.* **511**, 401 (2002).